Reports on Geodesy and Geoinformatics, 2026, Vol. 121, pp. 67–76

DOI: 10.2478/rgg-2026-0006
Received: 10 March 2026 / Accepted: 22 June 2026
Published online: 29 June 2026

ORIGINAL ARTICLE

Quantitative assessment of 2D-3D thematic convergence in UAV-based terrain inventory

Robert Gradka [1*] and Izabela Piech [2]

[1]Department of Geodesy and Geoinformatics, Wroclaw University of Science and Technology, Wybrzeże Stanisława Wyspiańskiego 27, 50-370, Wrocław, Poland
[2]Department of Agricultural Surveying, Cadastre and Photogrammetry, Faculty of Environmental Engineering and Geodesy, University of Agriculture in Krakow, Balicka 253a, 30-198, Kraków, Poland

*robert.gradka@pwr.edu.pl

Abstract

While geometric accuracy, expressed as Root Mean Square Error (RMSE), serves as the primary benchmark in Unmanned Aerial Vehicle (UAV) photogrammetry, thematic consistency between planar (2D) and volumetric (3D) deliverables remains insufficiently quantified. This study investigates the "accuracy paradox" questioning the assumption that high georeferencing precision inherently ensures thematic reliability. Research was conducted over a 22.6-hectare rural site in southern Poland. Using a UAV photogrammetric model (3 cm Ground Sampling Distance (GSD), 0.136 m RMSE), independent manual land-use delineations were performed on a high-resolution orthomosaic and a dense point cloud. To evaluate discrepancies, the Convergence Index (CI) was introduced, quantifying relative area differences between representations. Results indicate a total thematic discrepancy of 2.4% (0.5419 ha). However, errors were non-uniformly distributed: infrastructural classes showed near-perfect agreement (CI < 1%), whereas forested areas exhibited CI values exceeding 6%. 2D projections tended to overestimate forested areas, creating a false horizontal expansion of tree canopies. Furthermore, a strong negative correlation (Pearson $r = -0.95$, $p < 0.001$) was found between image overlap redundancy and thematic divergence. The study concludes that object morphology and 3D reconstruction completeness exert a more significant impact on inventory reliability than nominal georeferencing accuracy. For high-precision cadastral and environmental surveying, integrating 3D point clouds may be necessary, particularly in vegetation-dominated environments, to mitigate systematic distortions inherent in 2D orthomosaic projections.

Key words: UAV photogrammetry, thematic convergence, Convergence Index (CI), land-use mapping, Structure-from-Motion (SfM), geometric accuracy

1 Introduction

Validation of Unmanned Aerial Vehicle (UAV) photogrammetric deliverables has traditionally centered on geometric precision, typically quantified by Root Mean Square Error (RMSE) at Ground Control Points (GCPs). Research confirms that with optimized flight configurations and robust ground control strategies, UAV-based products consistently achieve centimeter-level positional accuracy (Agüera-Vega et al., 2017a; Stroner et al., 2020; Yildiz and Yaman, 2025). The stability and final precision of these models are heavily influenced by the number, spatial distribution, and reliability of GCPs (Agüera-Vega et al., 2017b; Yu et al., 2020; Cabo et al., 2021; Zhong et al., 2025). In elongated or corridor-type study areas, strategic GCP placement is vital for mitigating longitudinal distortions and ensuring uniform accuracy (Ferrer-González et al., 2020). Concurrently, the integration of Real-Time Kinematic (RTK)/Post-Processing Kinematic (PPK) positioning and high-precision onboard Global Navigation Satellite Systems (GNSS) has reduced the dependency on dense physical control networks while maintaining rigorous survey standards (Stroner et al., 2020, 2021; Martínez-Carricondo et al., 2023; Atik and Arkali, 2024).

Beyond positional metrics, the reliability of photogrammetric reconstruction is continuously enhanced by methodological improvements in Structure-from-Motion (SfM), which reconstruct

scene geometry indirectly from image correspondences and are therefore sensitive to image texture, visibility, and viewing geometry (Colomina and Molina, 2014), as well as camera modeling and anomaly detection during data acquisition (Meng et al., 2025). Recent findings by Tinkham and Woolsey (2024) highlighted the sensitivity of SfM-derived metrics to algorithm parameterization in vegetation-rich environments, while Wang et al. (2025) introduced non-parametric camera models to improve reconstruction stability in complex imaging geometries. These advancements in "point cloud intelligence" and automated data interpretation have significantly expanded the analytical potential of UAV datasets across land-use mapping, environmental monitoring, forestry inventory, and infrastructure planning (Yang et al., 2023; Wang et al., 2024; Bülbül et al., 2025; Liu et al., 2025; Sestras et al., 2025; Ivošević et al., 2025).

Despite this extensive body of research on geometric accuracy (Carrera-Hernández et al., 2020; Thuse, 2023; Malić et al., 2025), a critical gap remains regarding the quantitative consistency of thematic inventories derived from different photogrammetric representations generated from the same image block. Orthomosaics provide high planimetric clarity for land-use delineation, yet as a two-dimensional projection of RGB-based imagery they do not directly represent three-dimensional structure, which may lead to ambiguities in vertically complex objects such as vegetation (Stöcker et al., 2020; Sun et al., 2021; Karahan et al., 2025). Orthomosaics therefore lack the structural depth preserved in dense point clouds, as vertical information is collapsed during projection from 3D space to a 2D plane (Dronova et al., 2021). Variations in point density and local image overlap can introduce thematic boundary discrepancies, even when global geometric RMSE remains within acceptable limits (Sun et al., 2021; Dronova et al., 2021). Consequently, the extent to which planar and volumetric representations provide convergent thematic interpretations under operational survey conditions remains insufficiently quantified, particularly in complex terrain and vegetation-dominated environments (Karahan et al., 2025).

The objective of this study is to perform a quantitative assessment of thematic convergence between UAV-derived orthomosaics and dense point clouds in a rural terrain inventory. We introduce the Convergence Index (CI) as a formalized metric to express relative area differences between 2D and 3D interpretations. Our working hypothesis assumes that thematic divergence is primarily controlled by object morphology and reconstruction completeness rather than nominal georeferencing accuracy. By formalizing this 2D-3D agreement, the study aims to extend conventional accuracy assessment frameworks beyond positional error metrics toward a more rigorous evaluation of data convergence in geospatial applications.

2 Materials and methods

2.1 Study area

The research was conducted in a 22.6-hectare rural site in Starochęciny, Świętokrzyskie Voivodeship, Poland (see Fig. 1). The terrain is a representative agricultural-forest mosaic, featuring arable land, fallow areas, and dense forest patches. Its elongated geometry (corridor-like) increases sensitivity to flight configuration and ground control distribution, as noted in previous studies of linear surveys (Ferrer-González et al., 2020). To ensure high-quality reconstruction, the survey was executed under stable illumination conditions to minimize shadow-related artifacts.

2.2 UAV data acquisition

Data acquisition was performed using a GRYF unmanned aerial platform equipped with a Sony α6000 digital camera (24.3 MP, APS-C sensor). The flight was conducted at approximately 100 m above ground level, resulting in a mean ground sampling distance (GSD) of approximately 3 cm. Camera parameters were estimated through internal self-calibration during bundle adjustment.

The image block consisted of forty-five nadir photographs with forward overlap of at least 75% and side overlap not less than 60%, consistent with recommended configurations for high-quality orthomosaic generation (Stöcker et al., 2020). The survey was conducted using a nadir image acquisition geometry in a single-grid flight pattern adapted to the elongated shape of the study area.

Although forty-five images may appear to be a modest sample for a 22.6-hectare area, the combination of a 100 m flight altitude and a large APS-C sensor (24.3 MP) provided a substantial ground footprint per image. This ensured full terrain coverage while successfully maintaining the target 3 cm GSD, which allows for detailed object delineation and supports high-precision image-based measurements at the pixel level (Aasen et al., 2018). A linear, single-grid flight pattern was executed to best accommodate the elongated, corridor-like geometry of the site. Consequently, while the central longitudinal axis maintained high multi-view redundancy, this specific flight trajectory naturally resulted in a reduced overlap (3–4 images) along the lateral edges of the block.

Ground control was established in the Polish National Coordinate System PUWG 1992 (EPSG:2180). Ground control points were distributed across both boundary and internal parts of the study area to ensure geometric stability of the photogrammetric block.

Figure 2 illustrates the spatial arrangement of image footprints and control points. Their distribution was designed to minimize potential deformation in the elongated survey geometry.

2.3 Photogrammetric processing

Photogrammetric processing was conducted in Agisoft Metashape using a standard SfM and Multi-View Stereo (MVS) workflow (Turner et al., 2012; Colomina and Molina, 2014; Nex and Remondino, 2013).

The workflow included:

i. Image alignment and sparse point cloud generation,
ii. Bundle adjustment with GCP-based optimization,
iii. Dense point cloud reconstruction,
iv. Digital elevation model (DEM) generation,
v. Orthomosaic generation.

The applied workflow follows a standard and reproducible SfM-MVS processing scheme commonly used in UAV photogrammetry.

The orthomosaic is generated through the projection of the reconstructed three-dimensional surface onto a two-dimensional plane, which inherently removes vertical information and may introduce geometric distortions in areas with complex morphology (Turner et al., 2012).

Figure 3 presents the complete processing scheme from image acquisition to convergence analysis. The alignment process resulted in 13 259 tie points.

The spatial distribution of image overlap redundancy is presented in Figure 4. Central areas of the block were covered by 7–9 images, while boundary zones maintained a minimum overlap of three to four images. This level of multi-image coverage ensured sufficient geometric redundancy during bundle adjustment, particularly in the central part of the study area. Following optimization, the reprojection error reached 0.136 m. DEM with a spatial resolution of approximately 0.12 m was generated. The dense point cloud (Figure 5) contained 17502156 points, corresponding to an average density of 67 pts/m^2.

An orthomosaic (Figure 6) with a ground resolution of 0.03 m

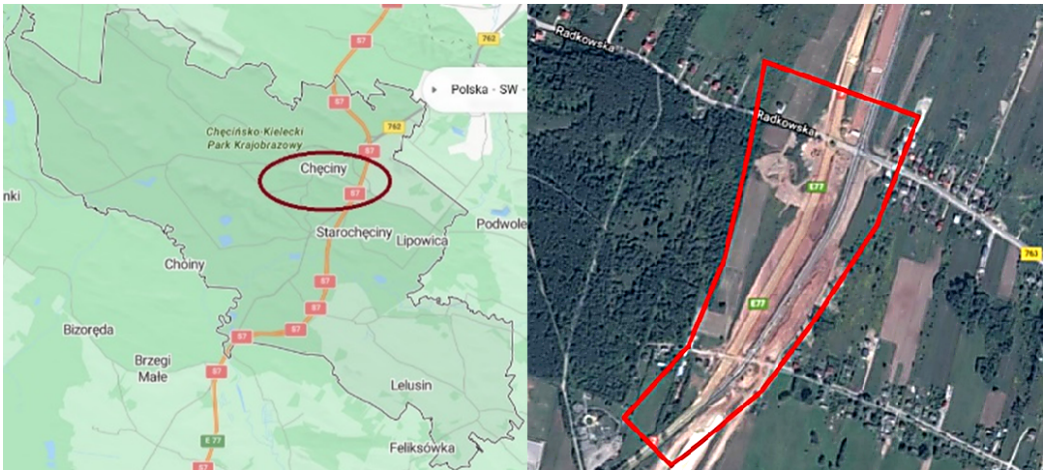

Figure 1. Location of Chęciny municipality within the Świętokrzyskie Voivodeship (left). Location of the surveyed area (right).

Figure 2. Spatial distribution of GCPs (used in adjustment – yellow) and CPs (independent validation – red) within the study area (Source: Own elaboration based on Widomski (2025))

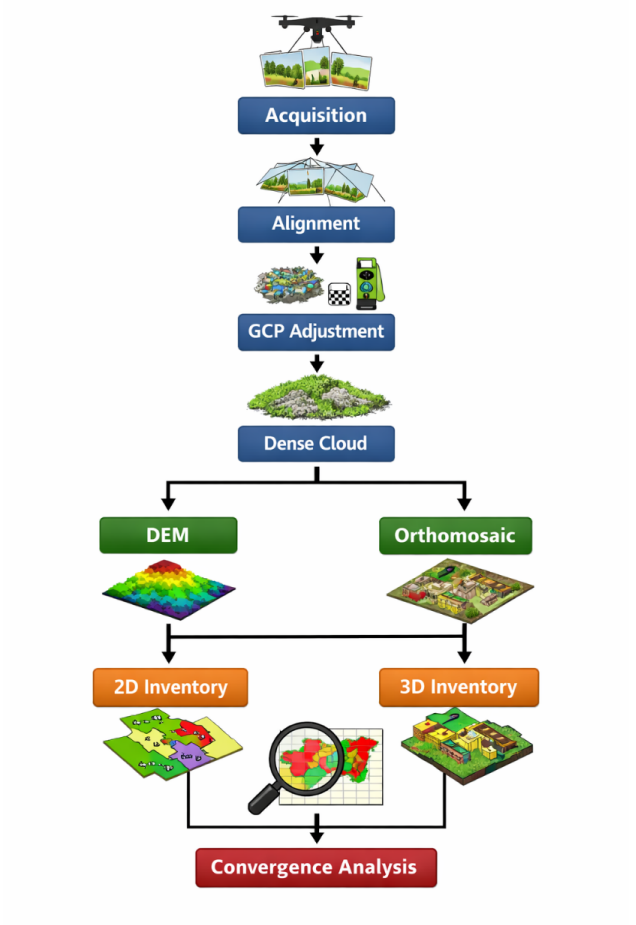

Figure 3. Workflow of UAV data processing and comparative 2D-3D inventory analysis

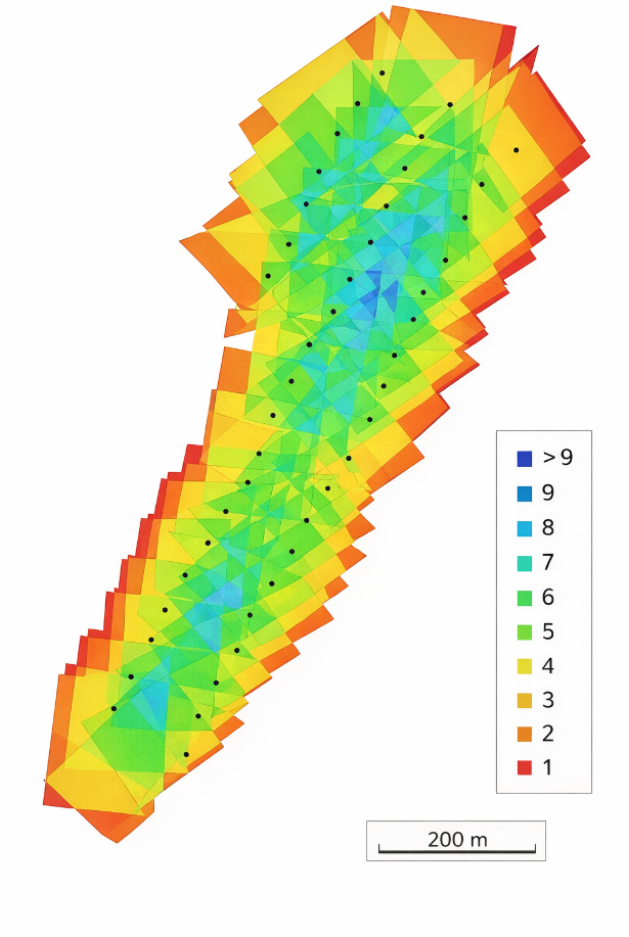

Figure 4. Spatial distribution of image overlap redundancy (number of images covering each area)

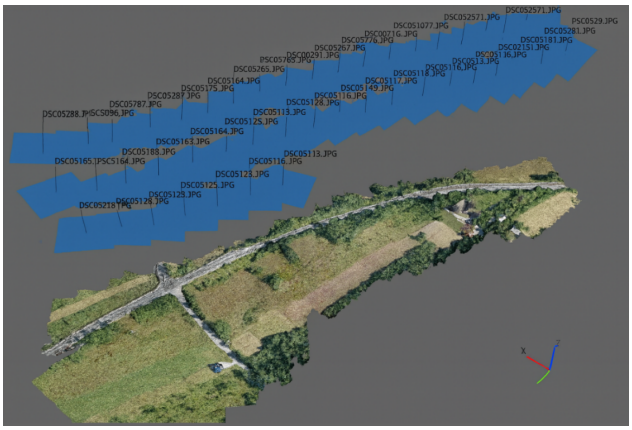

Figure 5. Dense point cloud (Source: Own elaboration based on Widomski (2025))

Figure 6. Fragment of the orthomosaic (3 cm GSD) illustrating boundary clarity of terrain objects (Source: Own elaboration based on Widomski (2025))

was produced for planar interpretation, acknowledging that such products represent a flattened projection of three-dimensional geometry (Turner et al., 2012).

2.4 Geometric accuracy assessment

The photogrammetric model was oriented using 4 GCPs, while three independent Check Points (CPs) were used exclusively for external validation, measured in the PUWG 1992 (EPSG:2180). The GCPs were distributed at the extremities of the elongated study area to ensure geometric stability of the photogrammetric block and to minimize potential deformation effects along its longitudinal axis. Each point was identified on a minimum of four overlapping images, providing sufficient geometric redundancy during bundle adjustment.

In addition to the adjustment points, three independent CPs were established for external accuracy validation. The CPs were not included in the bundle adjustment. Their spatial distribution was designed to represent varying overlap conditions within the block: one CP located in the central high-overlap zone (7–9 images), one in a medium-overlap area, and one near the block boundary characterized by reduced image redundancy (3–4 images).

The geometric quality of the photogrammetric model was evaluated using Root Mean Square Error (RMSE):

$$RMSE = \sqrt{\frac{\sum_{i=1}^{n}(X_{\text{model},i} - X_{\text{ref},i})^2}{n}} \quad (1)$$

Table 1. Geometric accuracy statistics of UAV-derived products

Product	Reprojection RMSE [m]	RMSE X [m]	RMSE Y [m]	RMSE Z [m]
Orthomosaic (2D)	0.093	0.067	0.071	–
Dense Point Cloud (3D)	0.136	0.082	0.089	0.191

Table 2. Geometric accuracy assessment based on GCP adjustment and independent CP validation

Dataset	RMSE XY [m]	RMSE Z [m]	Number of points
GCP (adjustment)	0.093	0.191	4
CP (validation)	0.101	0.208	3

where $X_{model,i}$ represents model-derived coordinates and $X_{ref,i}$ denotes reference coordinates of ground control points.

A separate RMSE was calculated for planimetric (X, Y) and vertical (Z) components based on differences between model-derived and reference coordinates.

Planimetric and vertical accuracy values derived from GCP adjustment and independent CP validation are summarized in Table 1 and Table 2.

The reprojection RMSE of the photogrammetric block reached 0.136 m, indicating stable bundle adjustment under the applied ground control configuration. For the orthomosaic (2D), planimetric accuracy expressed by RMSE amounted to 0.093 m, with RMSE X and RMSE Y equal to 0.067 m and 0.071 m, respectively. These values correspond to approximately three times the ground sampling distance (GSD ≈ 0.03 m), which is consistent with accuracy levels reported for UAV surveys conducted at similar flight altitudes (Agüera-Vega et al., 2017a; Stroner et al., 2020). For the dense point cloud (3D), horizontal accuracy components remained within the decimetre range, while the vertical component reached 0.191 m. The higher vertical RMSE is typical for UAV-SfM performance, where elevation accuracy is generally lower than planimetric precision due to image geometry (Yu et al., 2020; Zhong et al., 2025).

Independent validation using three CPs yielded a planimetric RMSE of 0.101 m and a vertical RMSE of 0.208 m. The close agreement between GCP-based and CP-based statistics confirms stable block geometry and the absence of systematic deformation.

Although several studies emphasize the importance of higher GCP numbers for optimizing global accuracy (Agüera-Vega et al., 2017b; Cabo et al., 2021; Yu et al., 2020; Zhong et al., 2025), the achieved RMSE of 0.136 m indicates stable block adjustment under the applied configuration.

Overall, the achieved geometric accuracy was considered sufficient for thematic terrain inventory purposes, particularly, given that the primary objective of this study was to evaluate relative thematic convergence between datasets rather than absolute geodetic precision.

2.5 Convergence Index definition

CI was used as the primary metric to quantify thematic agreement between 2D and 3D inventories:

$$CI = \frac{\left|A_{2D} - A_{3D}\right|}{\frac{1}{2}(A_{2D} + A_{3D})} \times 100\% \quad (2)$$

where:

A_{2D} – area derived from orthomosaic interpretation,
A_{3D} – area derived from dense point cloud interpretation.

CI values approaching zero indicate strong thematic consistency, while higher values represent increasing divergence between planar and volumetric representations.

Absolute area differences were additionally computed as:

$$\Delta A = A_{2D} - A_{3D} \quad (3)$$

This dual-metric approach allows for separation of geometric accuracy (RMSE) from thematic convergence (CI).

CI was selected as the primary metric for three main reasons: first, the inventories compared in this study were produced manually and independently without pixel-level co-registration of thematic boundaries. Therefore, boundary-based overlap metrics such as Intersection over Union (IoU) would introduce artificial sensitivity to minor edge displacements rather than reflecting overall thematic consistency. Second, the primary objective was to evaluate relative surface agreement at the class level rather than boundary precision. Third, CI provides a scale-independent, symmetric measure of divergence that directly expresses relative area discrepancy between representations. While mathematically related to classical normalized difference metrics, the novelty of CI lies in its application context: it is specifically designed to compare independently derived 2D and 3D thematic inventories where boundary alignment is not strictly enforced.

3 Results

3.1 Inventory area comparison

Land-use inventory was performed independently using orthomosaic (2D planar representation) and dense point cloud (3D volumetric representation). Twelve land-use classes were delineated using manual interpretation in MicroStation Power Draft V8i. Manual delineation ensured consistent interpretation criteria across both datasets and eliminated algorithm-dependent classification variability. The 3D dataset was analysed using RGB visualization and elevation shading to support boundary identification in areas of variable vegetation structure. Crucially, however, that manual navigation and boundary delineation within the 3D point cloud space was significantly more time-consuming and computationally demanding compared to traditional 2D digitization on the planar orthomosaic. The total surface area of the study site derived from orthomosaic-based interpretation amounted to 22.6351 ha, whereas the dense point cloud-based inventory resulted in a total area of 22.0932 ha.

The absolute difference between both representations reached 0.5419 ha, corresponding to 2.4% of the study area. However, a detailed analysis of Table 3 reveals a systematic overestimation of high-vegetation areas in the 2D planar projection. Specifically, the forest class area measured 3.1504 ha on the orthomosaic compared to 2.9548 ha in the 3D point cloud, indicating a planar overestimation of nearly 0.2 ha. This discrepancy arises because tree canopies projected onto a flat 2D plane obscure more ground area, creating a false horizontal expansion. The 3D point cloud, conversely, allows for a more accurate separation of vertical structures from the ground. In stark contrast, flat, infrastructural classes such as buildings exhibited near-perfect agreement (a difference of merely 0.0001 ha), confirming that 2D representations are generally sufficient and highly reliable for rigid, planar objects. The largest absolute area differences were observed for forest (0.1956 ha), fallow land (0.1551 ha), and tree stands (0.1277 ha). In contrast, infrastructural and built-up classes exhibited minimal discrepancies.

Figures 7 and 8 illustrate visual similarities between representations, particularly in planar objects such as roads and buildings.

Table 3. Comparison of land-use areas derived from orthomosaic (2D) and dense point cloud (3D)

Land-use class	**Area 2D** [ha]	**Area 3D** [ha]	**ΔA** [ha]	**Relative difference** [%]	**CI**
Arable land	4.9799	4.9465	0.0334	0.6700	0.0067
Meadows & pastures	0.4477	0.4562	-0.0085	1.9000	0.0188
Forest	3.1504	2.9548	0.1956	6.2100	0.0641
Tree stands	2.3258	2.1981	0.1277	5.4900	0.0566
Fallow land	7.7738	7.6187	0.1551	1.9900	0.0201
Greenery	1.2317	1.2049	0.0268	2.1800	0.0220
Water bodies	0.2124	0.2091	0.0033	1.5500	0.0157
Paved roads	0.8462	0.8391	0.0071	0.8400	0.0084
Improved unpaved roads	0.6875	0.6754	0.0121	1.7600	0.0178
Dirt roads	0.5663	0.5522	0.0141	2.4900	0.0252
Pedestrian paths	0.0893	0.0893	0.0000	0.0000	0.0000
Buildings	0.3241	0.3240	0.0001	0.0300	0.0003
Total	22.6351	22.0932	0.5419	2.4000	—

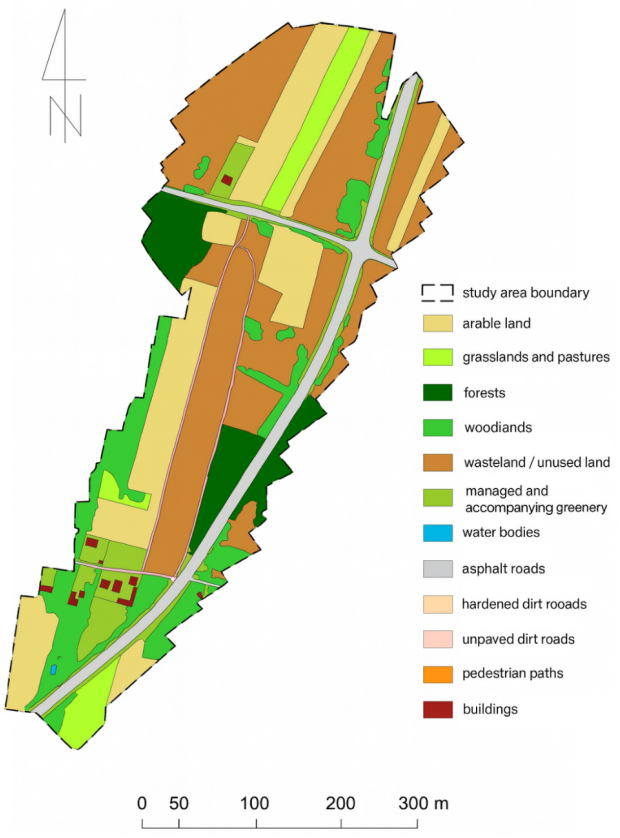

Figure 7. Terrain inventory map based on the dense point cloud (Source: Own elaboration based on Widomski (2025))

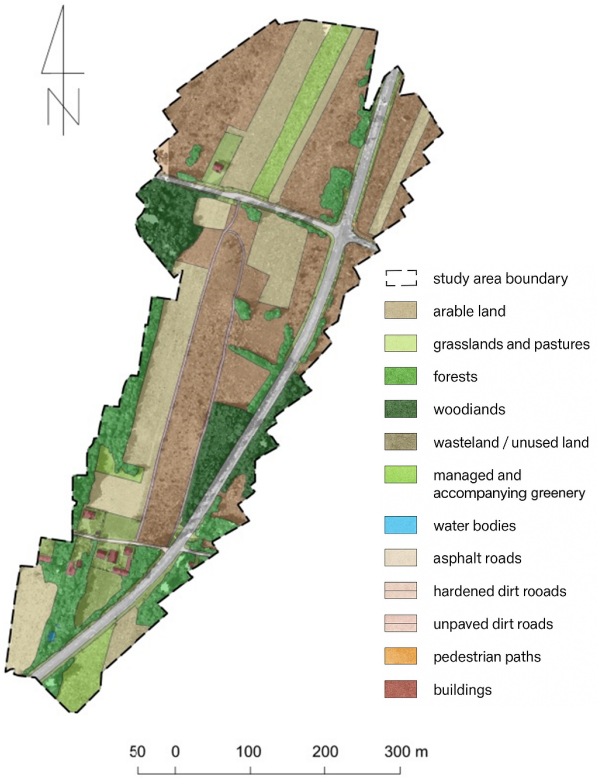

Figure 8. Terrain inventory map on the orthomosaic base (Source: Own elaboration based on Widomski (2025))

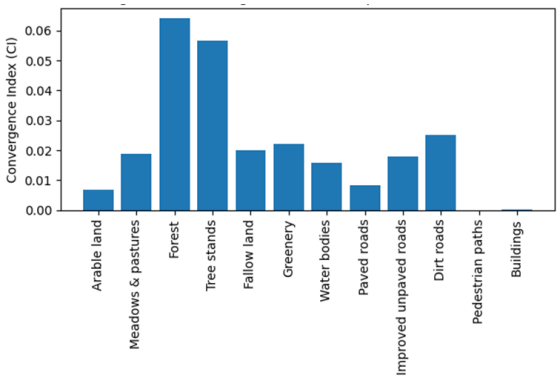

Figure 9. CI values per land-use class

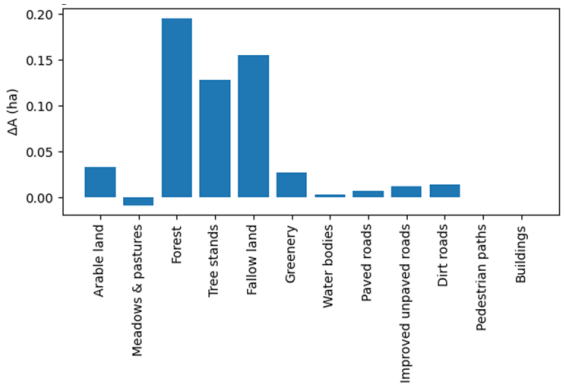

Figure 10. Absolute area differences between 2D and 3D inventories per land-use class

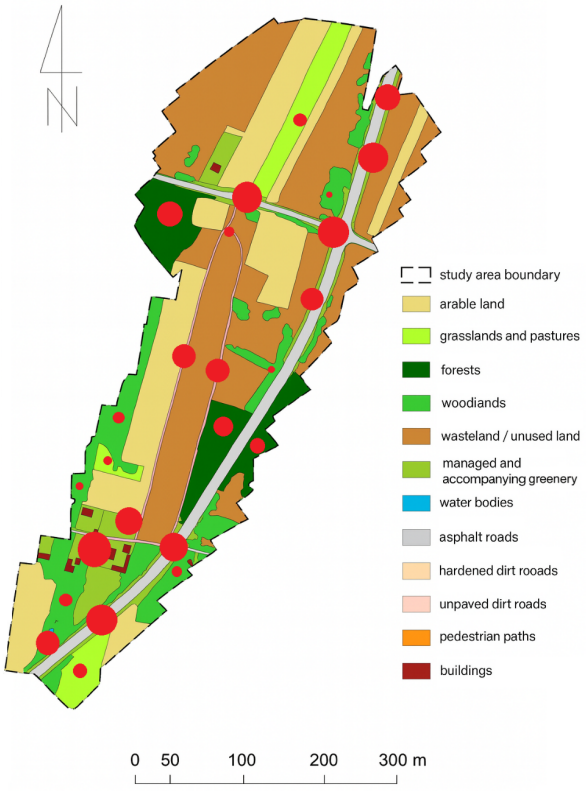

Figure 11. Difference map between inventories derived from the point cloud and the orthomosaic (differences indicated by red circles) (Source: Own elaboration based on Widomski (2025))

3.2 Convergence Index analysis

To evaluate thematic consistency independently from geometric RMSE, CI was calculated for each land-use class (Figure 9). CI values below 0.01 were recorded for buildings and pedestrian paths, indicating near-perfect agreement. Forest and tree stand classes exhibited the highest CI values (above 0.05), suggesting increased divergence between planar and volumetric interpretation. Absolute differences per class are presented in Figure 10.

3.3 Spatial distribution of discrepancies

Spatial analysis revealed that discrepancies (Figure 11) were not randomly distributed but concentrated primarily on:

- forested areas,
- zones of complex vegetation structure,
- edge-of-flight regions characterized by reduced point density.

4 Discussion

The results confirm that UAV photogrammetry enables high-resolution terrain inventory with substantial agreement between orthomosaic (2D) and dense point cloud (3D) representations. The overall discrepancy of 2.4% between inventories indicates strong thematic consistency under operational survey conditions. Although the total discrepancy of 2.4% appears relatively small, its non-uniform distribution across land-use classes indicates systematic, class-dependent divergence rather than random noise. However, class-specific differences demonstrate that positional accuracy alone does not fully explain thematic reliability.

4.1 The accuracy paradox: RMSE vs. thematic reliability

The achieved reprojection accuracy (0.136 m) aligns with established UAV benchmarks (Agüera-Vega et al., 2017a; Stroner et al., 2020; Yildiz and Yaman, 2025). However, our findings reveal a critical disconnect satisfactory RMSE values – validated by independent Check Points – do not inherently guarantee thematic convergence between 2D and 3D products. While block stability was confirmed, forest classes showed measurable surface divergence. This suggests that geometric metrics are blind to representation-specific errors, justifying the need for CI as a complementary quality indicator.

4.2 Impact of geometry and morphology

The spatial concentration of discrepancies in vegetation-rich and edge-of-flight zones (overlap redundancy < 4 images) confirms that reconstruction completeness dictates thematic reliability, which is consistent with the finding that complex terrain and heterogeneous land cover amplify discrepancies between planar and volumetric representations (Karahan et al., 2025). In elongated survey geometries, these "edge effects" amplify surface underestimation in 3D (Ferrer-González et al., 2020). While planar objects (roads, buildings) showed near-zero CI due to their distinct geometry, forest canopies introduced interpretative ambiguity, as two-dimensional projections tend to overestimate crown extent due to the absence of vertical structure representation, a limitation widely reported in UAV-based vegetation studies (Sun et al., 2021). The vertical variability and reconstruction noise inherent in volumetric modeling of vegetation (Sun et al., 2021; Tinkham and Woolsey, 2024) explain why orthomosaics, despite their 2D limitations, may offer more stable tonal boundaries for certain classes, whereas point clouds capture structural complexity at the cost of boundary noise (Yang et al., 2023; Wang et al., 2024). This sug-

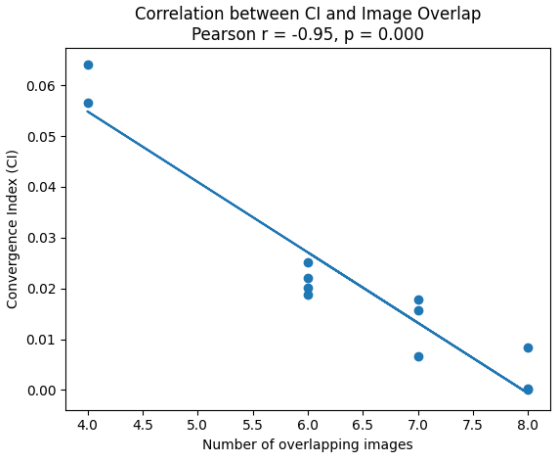

Figure 12. Relationship between image overlap redundancy (number of overlapping images) and CI values for individual land-use classes

gests that three-dimensional data sources, particularly, dense point clouds or LiDAR-derived datasets, are more suitable for representing vegetation structure in inventory applications than purely planar orthomosaics (Wallace et al., 2012).

To quantitatively assess the influence of reconstruction completeness on thematic divergence, the relationship between image overlap redundancy and class-level CI values was analysed (Figure 12). The overlap in redundancy per class was estimated as the dominant image coverage within areas representing a given land-use class. The overlap values ranged from 3–4 images in boundary zones to 7–9 images in central areas.

A strong negative correlation was observed (Pearson $r = -0.95$, $p < 0.001$, 95% CI: [−0.99, −0.81]), indicating that areas covered by fewer images tend to exhibit higher divergence between planar and volumetric inventories. Although the sample size ($n = 12$ land-use classes) is relatively small, it represents the complete, closed set of land-use categories present within the study area, making it sufficient for an exploratory statistical evaluation of this relationship. This provides strong empirical evidence that reduced image overlap – often implemented to optimize flight efficiency – negatively affects the thematic reliability of vegetation mapping, particularly, at the edges of the flight block and in structurally complex environments (Dronova et al., 2021). It should be noted that the relatively small number of images (45) and the resulting overlap distribution may have contributed to local reconstruction inconsistencies, particularly at block edges. However, this condition reflects realistic operational constraints in UAV surveys and therefore does not invalidate the observed 2D–3D divergence, but highlights its sensitivity to acquisition parameters. Even if the global geometric adjustment (RMSE) remains mathematically stable on ground control points, the localized lack of multi-image redundancy may introduce systematic distortion in 3D morphological reconstruction.

Overall, the observed discrepancies align with previous studies demonstrating that the limitations of 2D projections become increasingly significant in environments characterized by vertical complexity and heterogeneous surface structure (Sun et al., 2021; Karahan et al., 2025).

4.3 Robustness and sensitivity of the Convergence Index

To evaluate robustness of CI, a sensitivity analysis was performed assuming a conservative boundary interpretation tolerance equal to one pixel (0.03 m). The maximum potential surface variation attributable to boundary displacement was approximated as:

$$\Delta A_{max} = P \times t \tag{4}$$

where P denotes class perimeter and t represents boundary tolerance.

Even under this upper-bound assumption, estimated boundary-induced variation represented only a minor fraction of observed discrepancies for forest and tree stand classes. This indicates that divergence cannot be explained solely by minor boundary shifts.

The calculated $\Delta A_{\max}$ values were compared with observed absolute surface differences $\left|A_{2D} - A_{3D}\right|$. For infrastructural classes such as buildings and paved roads, the potential boundary-induced variation represented only a small fraction of the measured surface discrepancy, and CI values remained close to zero. For forest and tree stand classes, although the perimeter length is substantially larger, the observed divergence significantly exceeded the estimated tolerance-induced variation. This indicates that the higher CI values observed for vegetation-rich areas cannot be attributed solely to minor boundary displacement.

To verify stability across normalization schemes, a Relative Difference (RD) metric was additionally computed:

$$\mathrm{RD} = \frac{\left|A_{2D} - A_{3D}\right|}{A_{2D}} \tag{5}$$

The RD reached 6.21% for forest and 5.49% for tree stands, while infrastructural classes exhibited values below 0.05%. The agreement between CI and RD confirms that the divergence pattern is not dependent on a specific metric formulation but reflects systematic differences between planar and volumetric representations. Unlike intersection-based similarity measures such as the Jaccard index (IoU), which require pixel-level boundary alignment, CI evaluates proportional surface divergence and is therefore more suitable for independently derived inventories. Overall, the sensitivity analysis demonstrates that the Convergence Index is robust to minor boundary variability and effectively captures structural differences resulting from reconstruction completeness and object morphology.

4.4 Methodological implications

While UAV-SfM is often proposed as a replacement for traditional surveying (Carrera-Hernández et al., 2020; Malić et al., 2025), our results suggest that the choice between 2D and 3D deliverables should be task-specific. Extracting features directly from a 3D point cloud mitigates the systematic projection errors inherent in 2D orthomosaics; however, the 3D vectorization process is substantially more resource-intensive for the operator. Therefore, the proposed CI framework serves as a practical decision-making tool. It allows geospatial professionals to identify specific land-use classes (e.g., forests) where the additional effort of 3D processing is strictly necessary for accuracy, and rigid classes (e.g., roads, buildings) where rapid 2D orthomosaic digitization remains entirely sufficient and reliable.

These findings carry significant weight for geospatial practitioners, particularly in the realm of legal geomatics and cadastral surveying. While a 2.4% total discrepancy might seem acceptable for general land-use planning, relying solely on cost-effective 2D orthomosaics can lead to substantial errors when delineating legal property boundaries that intersect or run parallel to forested areas. If a legal boundary determination relies on the apparent edge of a forest canopy derived from a 2D projection, the resulting area bias could provoke legal and financial disputes. Therefore, high-precision environmental or cadastral inventories may require integration of 3D point cloud analysis and CI framework to identify zones where 2D projections systematically fail to reflect 3D terrain reality.

5 Conclusions

This study provides a quantitative assessment of the thematic consistency between UAV-derived orthomosaics (2D) and dense point clouds (3D). Based on a 22.6 ha rural inventory, the results demonstrate an "accuracy paradox": while a photogrammetric model may achieve high geometric precision (RMSE = 0.136 m), this metric alone does not guarantee thematic reliability across different data representations.

The total observed discrepancy of 0.5419 ha (2.4%) highlights a non-uniform distribution of interpretative errors. The near-perfect agreement in infrastructural classes contrasted heavily with significant divergence in forested zones (CI > 6%). Notably, 2D orthomosaics systematically overestimated vegetation boundaries due to the false horizontal expansion of projected canopies, confirming our hypothesis that thematic consistency is primarily governed by object morphology and reconstruction completeness rather than nominal georeferencing accuracy. This is quantitatively supported by a strong negative Pearson correlation ($r = -0.95$; $p < 0.001$) between image overlap redundancy and thematic divergence, indicating that reducing image overlap negatively affects 3D structural fidelity.

By introducing the CI, this research extends the standard UAV quality assessment framework beyond positional error metrics. The CI provides a robust, scale-independent tool for quantifying 2D-3D agreement, revealing localized thematic failures in areas of low overlap redundancy or complex vertical structures.

For geospatial practitioners, these findings carry significant weight. While 2D orthomosaics are planimetrically clear and sufficient for rigid infrastructure, relying on them in vegetation-rich environments introduces systematic area bias. In the context of high-precision legal and cadastral surveying, boundaries derived from 2D projections intersecting forested areas pose a critical risk of provoking property disputes. Therefore, high-precision cadastral or environmental surveys may require integration of 3D point cloud analysis, particularly in vegetation-dominated environments.

Future research should address the scalability bottleneck of manual delineation by applying the CI framework to automated classification workflows and further refine the methodology by incorporating spatial displacement metrics, such as Hausdorff distance, to capture geometric shifts alongside proportional area divergence.

6 Study limitations

Despite the robust patterns identified, several limitations of this study should be noted:

i. **Operator subjectivity**: Land-use delineation was performed manually in MicroStation Power Draft V8i. While intentionally chosen to eliminate algorithmic classification bias, this approach presents a significant scalability bottleneck. Delineating a 22.6-hectare site manually is feasible for a controlled study, but scaling this methodology to municipal or regional inventories (thousands of hectares) is operationally impractical. Future investigations should utilize the Convergence Index to compare manual delineations with automated classification workflows (Yang et al., 2023; Wang et al., 2024).

ii. **Environmental variables**: The research was conducted in a rural area with moderate topography. Convergence levels may vary in high-density urban environments or mountainous terrain, where extreme occlusions and vertical complexity could further amplify 2D-3D discrepancies.

iii. **Temporal variability**: The analysis was based on a single temporal dataset. Seasonal variability (e.g., leaf-on vs. leaf-off conditions) may influence 2D-3D convergence and should be investigated in future studies.

iv. **Validation data**: Geometric accuracy relied on bundle adjustment and GCP/CP configurations. While sufficient for RMSE assessment, the integration of independent, high-density ground truth data (e.g., Terrestrial Laser Scanning) would allow for a more granular analysis of the relationship between absolute positional truth and thematic consistency. The relatively small number of GCPs (4) and CPs (3) constitutes a limitation of the study and may affect the statistical robustness of RMSE-based validation. However, the primary objective of this research was not absolute geodetic accuracy but relative thematic comparison between datasets. Detailed coordinates and individual residuals of GCPs and CPs are available from the corresponding author upon request.

v. **Metric scope and spatial displacement**: The CI evaluates proportional surface divergence based on aggregated class areas rather than linear boundary displacement. Consequently, it does not explicitly capture spatial offsets; a theoretical scenario where a 1-hectare forest in 2D and a 1-hectare forest in 3D are perfectly equal in area but spatially displaced would still yield a CI of zero. To address this limitation, future methodological refinements should incorporate spatial boundary metrics, such as the Hausdorff distance. Unlike the CI, which focuses on aggregated proportional surface divergence, the Hausdorff distance measures the maximum distance between the closest points of two corresponding boundaries. Combining these two metrics would provide a comprehensive evaluation framework: utilizing the CI to detect representation-driven area inflation, and the Hausdorff distance to identify pure spatial offsets and boundary shifts.

These limitations do not invalidate the observed patterns but indicate that the results should be interpreted within the context of the experimental setup.

Acknowledgements

Part of the field reference data was collected during earlier research activities conducted under academic supervision and subsequently reanalysed for the purposes of this study.

Data availability

The datasets generated and analysed during the current study (including high-resolution orthomosaic and dense point clouds of the Starochęciny area) are not publicly available due to their large file size but are available from the corresponding author on reasonable request.

During the preparation of this manuscript, the authors used OpenAI solely to improve language quality, clarity, and editorial structure of the text. The tool was not used to generate scientific content, data, analyses, or conclusions. All text was subsequently reviewed and edited by the authors, who take full responsibility for the content of the article. In addition, selected figures were subjected to minor technical adjustments (e.g., contrast and brightness enhancement) to improve visual clarity, and textual elements within figures (labels and legends) were translated into English. These actions did not modify the underlying data, spatial extent, or interpretation of the results.

References

Aasen, H., Honkavaara, E., Lucieer, A., and Zarco-Tejada, P. J. (2018). Quantitative Remote Sensing at Ultra-High Resolution with UAV Spectroscopy: A Review of Sensor Technology, Measurement Procedures, and Data Correction Workflows. *Remote Sensing*, 10(7):1091, doi:10.3390/rs10071091.

Agüera-Vega, F., Carvajal-Ramírez, F., and Martínez-Carricondo, P. (2017a). Accuracy of Digital Surface Models and Orthophotos

Derived from Unmanned Aerial Vehicle Photogrammetry. *Journal of Surveying Engineering*, 143(2), doi:10.1061/(asce)su.1943-5428.0000206.

Agüera-Vega, F., Carvajal-Ramírez, F., and Martínez-Carricondo, P. (2017b). Assessment of photogrammetric mapping accuracy based on variation ground control points number using unmanned aerial vehicle. *Measurement*, 98:221–227, doi:10.1016/j.measurement.2016.12.002.

Atik, M. E. and Arkali, M. (2024). Comparative Assessment of the Effect of Positioning Techniques and Ground Control Point Distribution Models on the Accuracy of UAV-Based Photogrammetric Production. *Drones*, 9(1):15, doi:10.3390/drones9010015.

Bülbül, R., Reder, S., Berendt, F., Beiler, K., Cremer, T., and Mund, J.-P. (2025). Digital Forest Inventory Using Fused UAV and PLS Point Cloud Data. *The International Archives of the Photogrammetry, Remote Sensing and Spatial Information Sciences*, XLVIII-M-7-2025:299–304, doi:10.5194/isprs-archives-xlviii-m-7-2025-299-2025.

Cabo, C., Sanz-Ablanedo, E., Roca-Pardinas, J., and Ordonez, C. (2021). Influence of the Number and Spatial Distribution of Ground Control Points in the Accuracy of UAV-SfM DEMs: An Approach Based on Generalized Additive Models. *IEEE Transactions on Geoscience and Remote Sensing*, 59(12):10618–10627, doi:10.1109/tgrs.2021.3050693.

Carrera-Hernández, J. J., Levresse, G., and Lacan, P. (2020). Is UAV-SfM surveying ready to replace traditional surveying techniques? *International Journal of Remote Sensing*, 41(12):4820–4837, doi:10.1080/01431161.2020.1727049.

Colomina, I. and Molina, P. (2014). Unmanned aerial systems for photogrammetry and remote sensing: A review. *ISPRS Journal of Photogrammetry and Remote Sensing*, 92:79–97, doi:10.1016/j.isprsjprs.2014.02.013.

Dronova, I., Kislik, C., Dinh, Z., and Kelly, M. (2021). A Review of Unoccupied Aerial Vehicle Use in Wetland Applications: Emerging Opportunities in Approach, Technology, and Data. *Drones*, 5(2):45, doi:10.3390/drones5020045.

Ferrer-González, E., Agüera-Vega, F., Carvajal-Ramírez, F., and Martínez-Carricondo, P. (2020). UAV Photogrammetry Accuracy Assessment for Corridor Mapping Based on the Number and Distribution of Ground Control Points. *Remote Sensing*, 12(15):2447, doi:10.3390/rs12152447.

Ivošević, B., Pajević, N., Brdar, S., Waqar, R., Khan, M., and Valente, J. (2025). Comprehensive dataset from high resolution UAV land cover mapping of diverse natural environments in Serbia. *Scientific Data*, 12(1), doi:10.1038/s41597-025-04437-7.

Karahan, A., Demircan, N., Özgeriş, M., Gökçe, O., and Karahan, F. (2025). Integration of Drones in Landscape Research: Technological Approaches and Applications. *Drones*, 9(9):603, doi:10.3390/drones9090603.

Liu, X., De Cock, A., Ho, L., Pham, K., Panique-Casso, D., Forio, M. A. E., Maes, W. H., and Goethals, P. L. M. (2025). Mapping Waterbird Habitats with UAV-Derived 2D Orthomosaic Along Belgium's Lieve Canal. *Remote Sensing*, 17(15):2602, doi:10.3390/rs17152602.

Malić, B., Moser, V., Rajle, D., Kulić, S., and Barišić, I. (2025). Comparative Assessment of Vertical Precision of Unmanned Aerial Vehicle-Based Geodetic Survey for Road Construction: A Multi-Platform and Multi-Software Approach. *Infrastructures*, 10(11):287, doi:10.3390/infrastructures10110287.

Martínez-Carricondo, P., Agüera-Vega, F., and Carvajal-Ramírez, F. (2023). Accuracy assessment of RTK/PPK UAV-photogrammetry projects using differential corrections from multiple GNSS fixed base stations. *Geocarto International*, 38(1), doi:10.1080/10106049.2023.2197507.

Meng, C., Yang, H., Jiang, C., Hu, Q., and Li, D. (2025). Improving UAV Remote Sensing Photogrammetry Accuracy Under Navigation Interference Using Anomaly Detection and Data Fusion. *Remote Sensing*, 17(13):2176, doi:10.3390/rs17132176.

Nex, F. and Remondino, F. (2013). UAV for 3D mapping applications: a review. *Applied Geomatics*, 6(1):1–15, doi:10.1007/s12518-013-0120-x.

Sestras, P., Badea, G., Badea, A. C., Salagean, T., Roșca, S., Kader, S., and Remondino, F. (2025). Land surveying with UAV photogrammetry and LiDAR for optimal building planning. *Automation in Construction*, 173:106092, doi:10.1016/j.autcon.2025.106092.

Stroner, M., Urban, R., Reindl, T., Seidl, J., and Brouček, J. (2020). Evaluation of the Georeferencing Accuracy of a Photogrammetric Model Using a Quadrocopter with Onboard GNSS RTK. *Sensors*, 20(8):2318, doi:10.3390/s20082318.

Stroner, M., Urban, R., Seidl, J., Reindl, T., and Brouček, J. (2021). Photogrammetry Using UAV-Mounted GNSS RTK: Georeferencing Strategies without GCPs. *Remote Sensing*, 13(7):1336, doi:10.3390/rs13071336.

Stöcker, C., Nex, F., Koeva, M., and Gerke, M. (2020). High-Quality UAV-Based Orthophotos for Cadastral Mapping: Guidance for Optimal Flight Configurations. *Remote Sensing*, 12(21):3625, doi:10.3390/rs12213625.

Sun, Z., Wang, X., Wang, Z., Yang, L., Xie, Y., and Huang, Y. (2021). UAVs as remote sensing platforms in plant ecology: review of applications and challenges. *Journal of Plant Ecology*, 14(6):1003–1023, doi:10.1093/jpe/rtab089.

Thuse, T. (2023). *An assessment of UAV-generated digital elevation model using ground surveying techniques*. PhD thesis, Cape Peninsula University of Technology.

Tinkham, W. T. and Woolsey, G. A. (2024). Influence of Structure from Motion Algorithm Parameters on Metrics for Individual Tree Detection Accuracy and Precision. *Remote Sensing*, 16(20):3844, doi:10.3390/rs16203844.

Turner, D., Lucieer, A., and Watson, C. (2012). An Automated Technique for Generating Georectified Mosaics from Ultra-High Resolution Unmanned Aerial Vehicle (UAV) Imagery, Based on Structure from Motion (SfM) Point Clouds. *Remote Sensing*, 4(5):1392–1410, doi:10.3390/rs4051392.

Wallace, L., Lucieer, A., Watson, C., and Turner, D. (2012). Development of a UAV-LiDAR System with Application to Forest Inventory. *Remote Sensing*, 4(6):1519–1543, doi:10.3390/rs4061519.

Wang, M., Yue, G., Xiong, J., and Tian, S. (2024). Intelligent Point Cloud Processing, Sensing, and Understanding. *Sensors*, 24(1):283, doi:10.3390/s24010283.

Wang, Y., Pan, L., Pollefeys, M., and Larsson, V. (2025). Structure-From-Motion with a Non-Parametric Camera Model. In *2025 IEEE/CVF Conference on Computer Vision and Pattern Recognition (CVPR)*, page 1040–1049. IEEE, doi:10.1109/cvpr52734.2025.00105.

Widomski, M. (2025). Terrain inventory based on UAV imagery. Master's thesis, Faculty of Environmental Engineering and Geodesy, Hugo Kołłątaj University of Agriculture in Kraków, Poland.

Yang, B., Haala, N., and Dong, Z. (2023). Progress and perspectives of point cloud intelligence. *Geo-spatial Information Science*, 26(2):189–205, doi:10.1080/10095020.2023.2175478.

Yildiz, V. and Yaman, A. (2025). Comparison and accuracy assessment of unmanned aerial vehicle and terrestrial measurement in base map production. *The Egyptian Journal of Remote Sensing and Space Sciences*, 28(1):53–62, doi:10.1016/j.ejrs.2024.12.003.

Yu, J. J., Kim, D. W., Lee, E. J., and Son, S. W. (2020). Determining the Optimal Number of Ground Control Points for Varying Study Sites through Accuracy Evaluation of Unmanned Aerial System-Based 3D Point Clouds and Digital Surface Models. *Drones*, 4(3):49, doi:10.3390/drones4030049.

Zhong, H., Duan, Y., Tao, P., and Zhang, Z. (2025). Influence of ground control point reliability and distribution on UAV photogrammetric 3D mapping accuracy. *Geo-spatial Information Science*, 28(5):1998–2018, doi:10.1080/10095020.2025.2451204.